6-2014

Local Vibrational Modes Competitions in Mn-Doped ZnO Epitaxial Films with Tunable Ferromagnetism

Qiang Cao
Shandong University

Maoxiang Fu
Shandong University

Guolei Liu
Shandong University

Huaijin Zhang
Shandong University

Shishen Yan
Shandong University

See next page for additional authors

Citation Details

Cao, Q., Fu, M., Liu, G., Zhang, H., Yan, S., Chen, Y., ... & Jiao, J. (2014). Local vibrational modes competitions in Mn-doped ZnO epitaxial films with tunable ferromagnetism. Journal of Applied Physics, 115(24), 243906.

Authors
Qiang Cao, Maoxiang Fu, Guolei Liu, Huaijin Zhang, Shishen Yan, Yanxue Chen, Liangmo Mei, and Jun Jiao

Local vibrational modes competitions in Mn-doped ZnO epitaxial films with tunable ferromagnetism

Qiang Cao,[1,2] Maoxiang Fu,[1] Guolei Liu,[1,a)] Huaijin Zhang,[1] Shishen Yan,[1] Yanxue Chen,[1] Liangmo Mei,[1] and Jun Jiao[3]
[1]National Key Laboratory of Crystal Materials and School of Physics, Shandong University, Jinan, Shandong 250100, People's Republic of China
[2]School of Physics and Engineering, Qufu Normal University, Qufu, Shandong 273165, People's Republic of China
[3]Department of Mechanical and Materials Engineering, Portland State University, P.O. Box 751, Portland, Oregon 97207-0751, USA

(Received 5 May 2014; accepted 14 June 2014; published online 26 June 2014)

We reported spectroscopic investigations of high quality Mn-doped ZnO (ZnMnO) films grown by oxygen plasma-assisted molecular beam epitaxy. Raman scattering spectra revealed two local vibrational modes (LVMs) associated with Mn dopants at 523 and 712 cm^{-1}. The LVMs and magnetic properties of ZnMnO films can be synchronously modulated by post annealing processing or by introducing tiny Co. The relative intensity of two LVMs clearly shows competitions arising from uncompensated acceptor and donor defects competition for ferromagnetic and nonmagnetic films. The experimental results indicated that LVM at 523 cm^{-1} is attributed to Mn—(Zinc-vacancy) complexes, while LVM at 712 cm^{-1} is attributed to Mn—(Oxygen-vacancy) complexes. © *2014 AIP Publishing LLC*.
[http://dx.doi.org/10.1063/1.4885735]

I. INTRODUCTION

ZnO and related compounds have been receiving much attention over the past decades due to many existing or emerging applications in optoelectronics, transparent electronics, and spintronics.[1] To optimize their applications, it is essential to understand the behavior of defects since most of the properties depend in one way or another on the defects that are present in the material. Recently, a growing number of theoretical and experimental works have given an indication that defects play a primary role in mediating the ferromagnetism of transition-metal-doped ZnO.[2,3] In the case of Mn-doped ZnO (ZnMnO), although a large number of works on defect induced ferromagnetism are available in literature, an experimental evidence of direct link between defects and magnetic properties is still lacking. To clarify the detailed picture of defects in tailoring magnetic properties, it is very helpful to perform spectroscopic investigations on defects in materials, whose magnetic properties can be modulated. In particular, the characterization of local vibration of defects can yield very valuable information on the microstructure and nature of defects in materials, which has been demonstrated in Mg-doped and ion-implanted GaN.[4,5] However, no detailed investigations on local vibrational modes (LVMs) of defects and dopants have been reported, and the assignment of the LVMs in ZnMnO still remains a controversy.[6,7]

In this work, we presented spectroscopic investigations on ZnMnO epitaxial films with tunable ferromagnetism. The preparation of high-quality epitaxial films can availably avoid grain boundaries[8] or magnetic secondary phase,[9] which have great impact on the characterization of Raman scattering and magnetic properties. The ferromagnetism in ZnMnO films can be modulated by either thermal annealing processing or introducing tiny Co. Raman spectra revealed two LVMs at 523 and 712 cm^{-1}, which are related not only to Mn dopants but also to defects. The experimental results obtained from magnetic, photoluminescence, and Raman measurements indicated that LVM at 523 cm^{-1} is attributed to Mn—(Zinc-vacancy) complexes, while the LVM at 712 cm^{-1} is attributed to Mn—(Oxygen-vacancy) complexes.

II. EXPERIMENTAL

Three sets of samples were prepared and investigated: (1) as-prepared $Zn_{1-x}Mn_xO$ epitaxial films with Mn content $x = 0$, 0.01, 0.03, and 0.05. (2) Post-annealed $Zn_{1-x}Mn_xO$ ($x = 0$, 0.05) films. To compare the annealing effects, the sample at size of $5 \times 10\ mm^2$ was cut into 4 pieces. The first piece was annealed at 800 °C under ultra high vacuum (UHV) for an hour (UHV-anneal), the second one was annealed at 800 °C for an hour under UHV with irradiation of atomic oxygen flux by using an Oxford plasma source (O-anneal), and third one was annealed at 800 °C for an hour under UHV with irradiation of Zn flux by using a Zn k-cell (Zn-anneal), respectively. (3) $Zn_{0.99-x}Co_{0.01}Mn_xO$ epitaxial films with $x = 0$, 0.01, 0.03, and 0.05.

High quality ZnMnO films were grown on Al_2O_3 (0001) substrates by oxygen plasma-assisted molecular beam epitaxy (OPAMBE). The growth procedure has been described elsewhere.[10] The film growth was monitored by real time Reflection High Energy Electron Diffraction (RHEED). The crystal structure of epitaxial films was characterized by high resolution X-ray diffraction (HRXRD). The magnetic field dependent magnetization (M-H) curves were measured by an alternatively gradient magnetometer (AGM) at room

a)Author to whom correspondence should be addressed. Electronic mail: liu-guolei@sdu.edu.cn

temperature and by a superconductivity quantum interference device at low temperature. The Photoluminescence (PL) spectra were excited by a 325 nm He–Cd laser. The radiation of 514.53 nm from an Ar^+ ion laser with a total power of 10 mW was used as an excitation source, and it was focused to ~2 μm in diameter on the samples. The line positions were determined using a triple-grating monochromator with resolution better than 1 cm^{-1} in the wavenumber range from 200 to 1000 cm^{-1}.

III. RESULTS AND DISCUSSION

A. Epitaxial growth and Structural characterization

Fig. 1(a) shows the RHEED patterns for ZnO buffer layer, $Zn_{0.95}Co_{0.01}O$, $Zn_{0.95}Mn_{0.05}O$, and $Zn_{0.94}Co_{0.01}Mn_{0.05}O$ epilayers. The $ZnO/Al_2O_3(0001)$ buffer layer has stripe RHEED pattern, which displays layer by layer growth mode and smooth surface morphology. The elongated diffraction spots in Mn (or/and Co) doped ZnO films indicated a rougher surface morphology, which were caused by the doping induced distortion when part of the Zn cations was substituted by Mn or/and Co cations. Since RHEED is very sensitive to surface structure during film growth, no polycrystalline rings or surface structure other than ZnO were detected in doped ZnO films. Fig. 1(b) shows the HRXRD θ–2θ scans for $Zn_{0.95}Co_{0.01}O$, $Zn_{0.95}Mn_{0.05}O$, and $Zn_{0.94}Co_{0.01}Mn_{0.05}O$ films, only (0002) and (0004) peaks of wurtzite lattice were detected, which indicate all the doped films exhibit a single crystalline characteristic without any second phase. Furthermore, a full-width at half maximum of 0.295° in ω-rocking curves indicates high structural perfection in $Zn_{0.95}Mn_{0.05}O$ film.

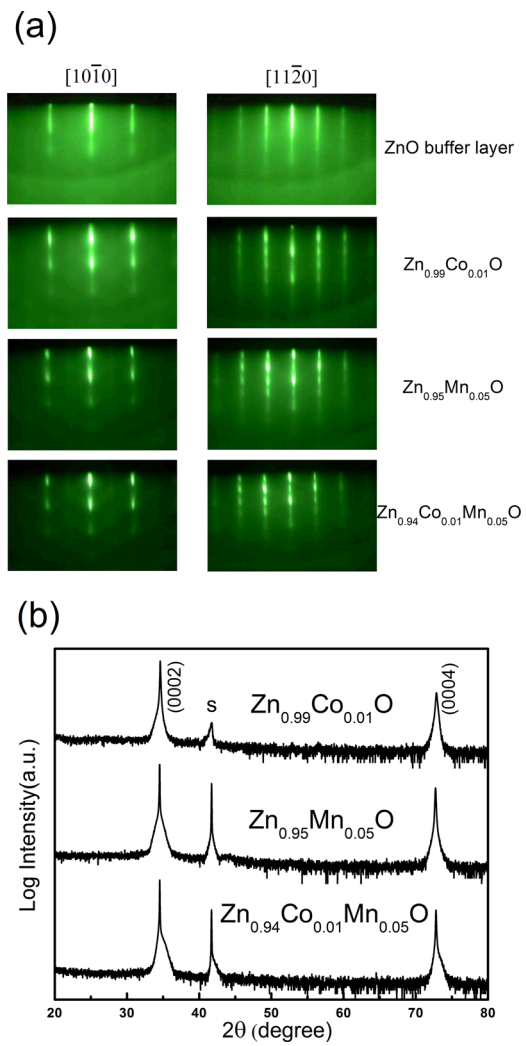

FIG. 1. (a) RHEED patterns for ZnO buffer layer, $Zn_{0.95}Co_{0.01}O$, $Zn_{0.95}Mn_{0.05}O$, and $Zn_{0.94}Co_{0.01}Mn_{0.05}O$ epilayers with the electron beam along ZnO [10$\bar{1}$0] (left column) and [11$\bar{2}$0] (right column) directions. (b) HRXRD θ–2θ scans for $Zn_{0.95}Co_{0.01}O$, $Zn_{0.95}Mn_{0.05}O$, and $Zn_{0.94}Co_{0.01}Mn_{0.05}O$ films. The peak from the sapphire substrate is denoted S.

B. Raman spectra of as-prepared films

Fig. 2 shows the Raman spectra of as-prepared $Zn_{1-x}Mn_xO$ epitaxial films with Mn content x = 0, 0.01, 0.03, and 0.05. For undoped ZnO film, the dominated $E_{2(high)}$ mode at 437 (I_2) cm^{-1} indicates an excellent crystalline of wurtzite ZnO lattice. In addition, there are four Raman-active vibration modes at 276 (I_1), 508 (I_4), 580 (I_6), and 642 (I_7) cm^{-1}, which are assigned to the $B_{1(low)}$, $2B_{1(low)}$, $B_{1(high)}$, and $TA + B_{1(high)}$ symmetric phonon modes,[11–13] respectively. The silent B_1 modes and the second-order modes observed in pure ZnO film are attributed to disorder-activated Raman scattering caused by growth conditions. For as-prepared $Zn_{1-x}Mn_xO$ films, with increasing Mn content, the intensity of disorder-activated phonon modes at 276 (I_1), 472 (I_3), 580 (I_6), and 642 (I_7) cm^{-1} enhances whereas the intensity of $E_{2(high)}$ (I_2) mode almost remains constant, which suggests that Mn ions substituted into wurtzite ZnO without destroying the host lattice. It should be noted that there are two addition modes (AMs): a peak at 712 (I_8) cm^{-1} and a broad peak around 523 (I_5) cm^{-1}. The mode around 523 cm^{-1} has been observed in most $Zn_{1-x}Mn_xO$ materials, but the assignment of this mode still remains a controversy.[6,7,14] The mode I_8 has not yet been reported in literature. It cannot be attributed to secondary phases, such as $ZnMn_2O_4$,[15] MnO_2,[16] Mn_2O_3,[16,17] and Mn_3O_4.[17] It is found that the AMs I_5 and I_8 are absent in pure ZnO films and Co doped ZnO films under

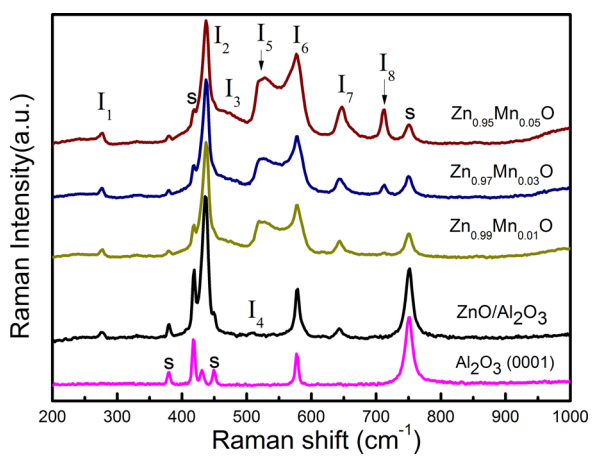

FIG. 2. Raman spectra of as-prepared $Zn_{1-x}Mn_xO$ epitaxial films with Mn content x = 0, 0.01, 0.03, and 0.05, as well as the referenced $Al_2O_3(0001)$ substrate. The vibration modes from substrate were marked by S.

the same growth conditions.[18] But both of them are observed in (Mn, Co) codoped ZnO films (Fig. 6). Further, the intensity of AMs I_5 and I_8 both increases with Mn content. Therefore, the AMs I_5 and I_8 are LVMs associated with Mn ions in ZnO lattice.

C. Effects of post-annealing

Fig. 3(a) shows the M-H curves for as-prepared, post-anneal $Zn_{0.95}Mn_{0.05}O$ films. As-prepared $Zn_{1-x}Mn_xO$ films are paramagnetic (PM) from room temperature until down to 5 K, which is consistent with the results reported in high-quality samples.[19,20] The Zn-anneal and UHV-anneal samples are both paramagnetic, whereas the O-anneal sample exhibits ferromagnetism (FM) at room temperature, which is clearly illustrated in Fig. 3(a). The surface and crystal structure after annealing treatments was re-checked by RHEED and HRXRD, which indicated that the O-anneal process improves the surface roughness and crystal quality of the samples. In addition, compared experiments using undoped ZnO films did not show ferromagnetism under any conditions. Fig. 3(b) shows the low temperature near-band PL spectra for annealed samples. Four PL peaks at 3.376, 3.357, 3.321, and 3.316 eV are observed, which correspond to recombinations of free exciton (FX),[21,22] neutral donor-bound exciton (D^0X),[21,23] neutral acceptor-bound exciton (A^0X),[23,24] and the first replica of FX,[25,26] respectively. The PL spectra clearly indicated the modulation of D^0X and A^0X emissions by annealing processing. The A^0X emission is dominated in the O-anneal film, whereas the D^0X emission is dominated for as-prepared, UHV-anneal, and Zn-anneal films. In addition, the RT Hall effect measurements revealed that post-annealing treatments strongly influence the resistivity of the samples. All the films are n-type conduction. The carrier concentrations are $9.0 \times 10^{17}\,cm^{-3}$, $2.1 \times 10^{18}\,cm^{-3}$, and $1.0 \times 10^{17}\ cm^{-3}$ for as-grown, Zn-anneal, and O-anneal films, respectively. The Hall measurements indicated that the O-anneal process reduces the n-type character of the material, which is consistent with the PL results. The above results revealed that the ferromagnetism activated by O-anneal processing arises from the uncompensated acceptor defects, which is consistent with theoretical predictions[27] and experimental results reported earlier.[28,29] Without incorporating any additional chemical impurities, the most possible effect of O-annealing is the cancellation of native oxygen vacancies, which may reduce the n-type character of the material and eventually allow some previously compensated native acceptor defects to hybridize with Mn ions and mediate the ferromagnetic coupling.

Fig. 4(a) shows the Raman spectra of as-prepared and post-annealed $Zn_{0.95}Mn_{0.05}O$ epitaxial films. In fact, Raman

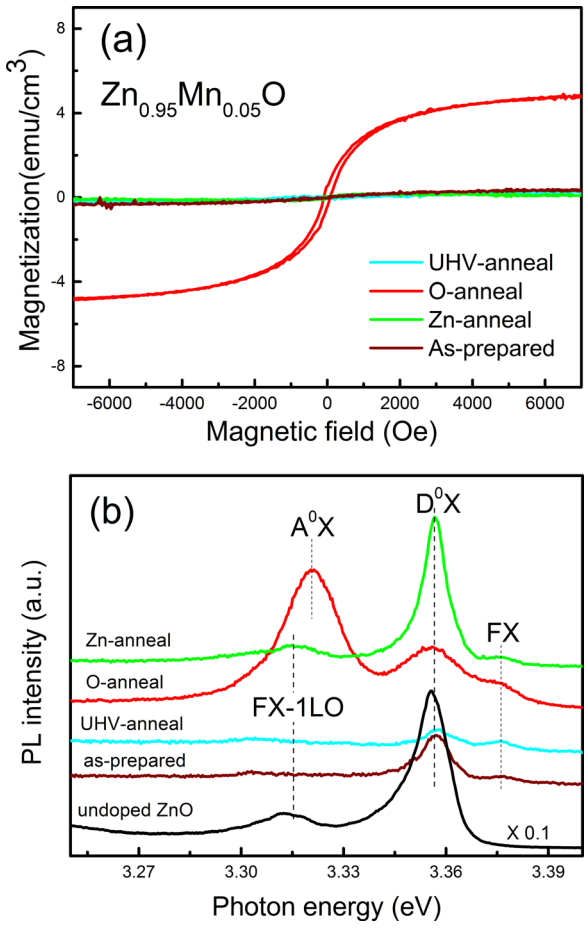

FIG. 3. (a) M-H curves of as-prepared, UHV-anneal, O-anneal, and Zn-anneal $Zn_{0.95}Mn_{0.05}O$ films at RT. (b) Near band PL spectra at 5 K for as-prepared, UHV-anneal, Zn-anneal, and O-anneal $Zn_{0.95}Mn_{0.05}O$ epitaxial films, as well as undoped ZnO film for comparison. The dashed lines are guides to the eyes.

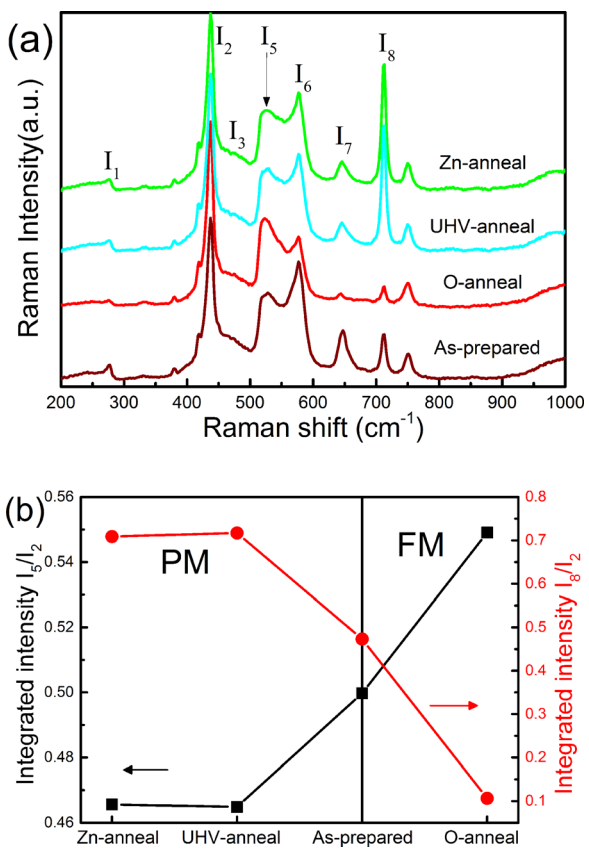

FIG. 4. (a) Raman spectra of as-prepared, O-anneal, UHV-anneal, and Zn-anneal $Zn_{0.95}Mn_{0.05}O$ epitaxial films. (b) Integrated intensity of I_5/I_2 and I_8/I_2 for as-prepared, Zn-anneal, UHV-anneal, and O-anneal $Zn_{0.95}Mn_{0.05}O$ epitaxial films.

scattering spectroscopy is very sensitive to the formation of secondary phases. It has been used as a powerful tool to detect many probable secondary phases in the host materials that may not be detectable by conventional XRD.[30] Besides the general appearance of the phonon modes observed in as-prepared samples, there are no additional modes attributed to the formation of magnetic secondary phases in post-annealed films. It indicates that post-annealed process did not introduce any secondary phase. It is interested that the integrated intensity of LVMs I_5 and I_8 are modulated by different annealing processing. By using Lorentz fitting, the integrated intensity of I_5/I_2 and I_8/I_2 for as-prepared, UHV-anneal, Zn-anneal, and O-anneal $Zn_{0.95}Mn_{0.05}O$ epitaxial films are shown in Fig. 4(b). The integrated intensity of I_8/I_2 is suppressed in O-anneal films, while it is enhanced in Zn-anneal or UHV-anneal films. Reversely, the integrated intensity of I_5/I_2 is enhanced in O-anneal sample, while it is depressed in Zn-anneal or UHV-anneal samples. The competition of LVMs indicates that they are related not only to Mn dopants but also to the defects in the material. Moreover, the results from PL measurements reveal that LVM I_5 associate with acceptor defects, while the LVM I_8 associates with donor defects. The dominated native acceptor defects in ZnO films are Zinc-vacancy or interstitial-oxygen. First-principles calculation showed that Zinc-vacancy has lowest formation energy.[31,32] In fact, Zinc-vacancy have been identified as the dominant compensating center in n-type ZnO by positron annihilation measurements,[33] and they are also more favorable in oxygen-rich conditions.[32] On another hand, the O_i at the tetrahedral site is unstable[32] and, spontaneously, relaxes through recombination with their vacancies upon thermal annealing. Therefore, Zinc-vacancy or their complexes are considered to be the dominant acceptor defects in our films. Among the defects behaved as donors, Oxygen-vacancy has the lowest formation energy,[31] and is more favorable under our oxygen deficient growth condition. In addition, Zinc interstitials have high formation energy and diffuse fast due to their migration barrier as low as 0.57 eV.[32] They are easily annealed out under our thermal annealing condition with the temperature up to 800 °C. Consequently, LVM I_5 can be attributed to local vibration of Mn—(Zinc-vacancy) complexes, while LVM I_8 can be attributed to local vibration of Mn—(Oxygen-vacancy) complexes.

D. Effects of (Mn, Co)-codoping

To confirm the assignment of LVMs I_5 and I_8, we studied Co-doped and (Mn, Co)-codoped ZnO epitaxial films, which were grown under similar conditions. Codoping[34,35] has been considered as a possible way to tailor the magnetic features of oxide magnetic semiconductors as a result of the existence of optimum structural dopant-defect configurations. Fig. 5 shows the M-H curves of $Zn_{0.99-x}Co_{0.01}Mn_xO$ epitaxial films with $x = 0$, 0.01, 0.03, and 0.05. Clear hysteresis loops are observed in samples with $x = 0.03$ and 0.05, which indicates that the ferromagnetism was switched on by introducing 1% Co. It is noticed that the $Zn_{0.99}Co_{0.01}O$ and $Zn_{1-x}Mn_xO$ epitaxial films are both paramagnetic. The fact that the saturated magnetization increases linearly with Mn content, as shown in the inset of Fig. 5, virtually eliminates the possibility of Co or cobalt oxide clusters being responsible for ferromagnetism. The ferromagnetic ordering in codoped samples is likely developed by the synergetic interactions.[35] It can be described as dopant-defect hybridization, i.e., $Mn^{2+} + Co^{2+} \rightarrow (Mn^{2+} + h^+_{acceptor})^{3+} + (Co^{2+} + e^-_{donor})^+$.[36,37] When additional Co dopants were introduced, more Mn—acceptor complexes were activated with increasing of Mn content, thereby the ferromagnetism was enhanced with Mn content. In this regard, the effect of the codoping is similar to O-anneal processes. As a consequence, the same trend should also be observed in Raman spectra for $Zn_{0.99-x}Co_{0.01}Mn_xO$ films.

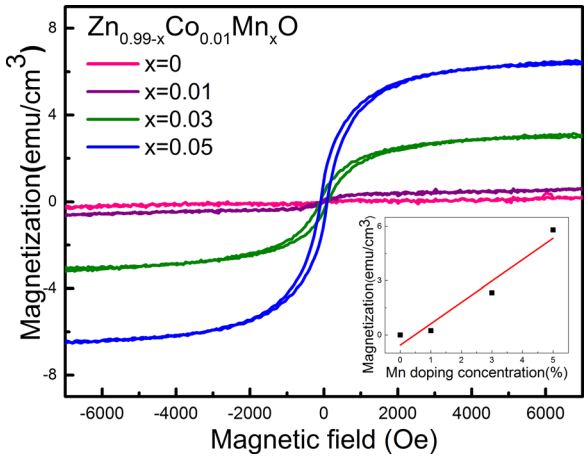

FIG. 5. M–H curves of $Zn_{0.99-x}Co_{0.01}Mn_xO$ films with $x = 0$, 0.01, 0.03, and 0.05. The inset shows the saturated magnetization as a function of Mn component.

Fig. 6(a) shows the Raman scattering spectra of $Zn_{0.99-x}Co_{0.01}Mn_xO$ epitaxial films. Figs. 6(b) and 6(c) show the integrated intensity of I_5/I_2 and I_8/I_2 as function of Mn content x for $Zn_{1-x}Mn_xO$ and $Zn_{0.99-x}Co_{0.01}Mn_xO$ epitaxial films, respectively. Although the integrated intensity of I_5 and I_8 are both enhanced with increasing Mn contents, the integrated intensity of I_5/I_2 was enhanced, while the integrated intensity of I_8/I_2 is suppressed for the $Zn_{0.99-x}Co_{0.01}Mn_xO$ by introducing 1% Co. The enhancement of I_5/I_2 and suppression of I_8/I_2 are consistent with the observation in O-anneal films as shown in Fig. 4, and further corroborate the assignments of LVM I_5 and I_8. Our previous work indicated that the mode I_9 is assigned to a cobalt-elemental sensitive mode.[18] The intensity of mode I_9 remains constant, which is consistent with the fixed concentration of Co (1%).

IV. SUMMARY

In summary, the magnetic, vibrational, and photoluminescence properties of high quality ZnMnO films grown by OPAMBE were studied. The ferromagnetism can be switched on in ways of oxygen annealing processing and introducing tiny Co. PL spectra of annealed samples indicated that the acceptor defects are dominant in O-anneal samples, whereas donor defects are dominant in other samples. Raman scattering spectra revealed two local vibrational modes (LVMs) associated with Mn dopants at 523 and 712 cm^{-1}. The relative intensity of two LVMs clearly shows

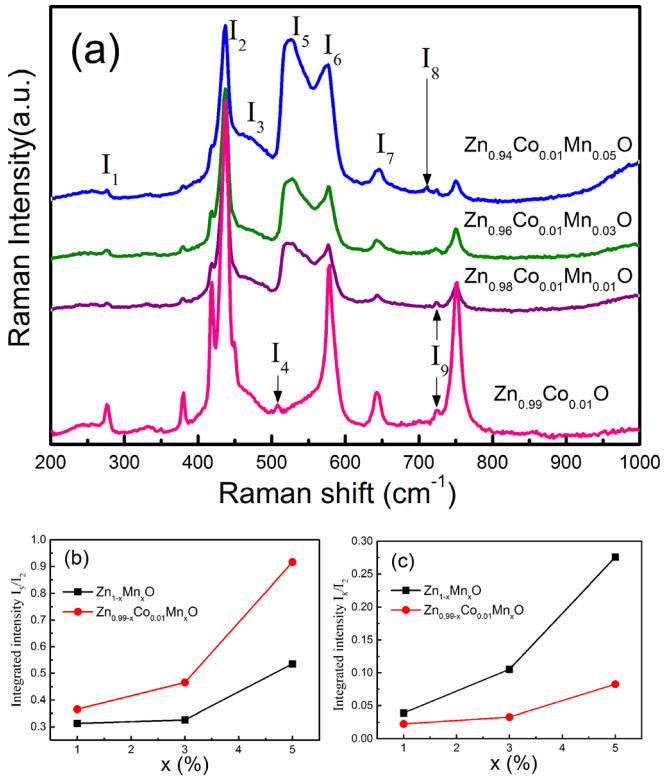

FIG. 6. (a) Raman spectra of $Zn_{0.99-x}Co_{0.01}Mn_xO$ epitaxial films with $x = 0.01$, 0.03, and 0.05, as well as the $Zn_{0.99}Co_{0.01}O$ film. (b) Integrated intensity of I_5/I_2 as a function of Mn content x for $Zn_{1-x}Mn_xO$ and $Zn_{0.99-x}Co_{0.01}Mn_xO$ epitaxial films. (c) Integrated intensity of I_8/I_2 as a function of Mn content x for $Zn_{1-x}Mn_xO$ and $Zn_{0.99-x}Co_{0.01}Mn_xO$ epitaxial films.

competitions arising from uncompensated acceptor to donor defects competition for ferromagnetic and nonmagnetic films. Our experimental results indicated that the LVM at 523 cm^{-1} is attributed to Mn—(Zinc-vacancy) complexes, and the LVM at 712 cm^{-1} is attributed to Mn—(Oxygen-vacancy) complexes.

ACKNOWLEDGMENTS

This work was financially supported by the State Key Project of Fundamental Research of China under Grant No. 2013CB922303, the NSF Grant Nos. 11374189 and 51231007, 111 Project B13029, Shandong Postdoctoral Grant No. 201303099, Research Grants from China Electronics Technology Group Corporation No. 46 Research Institute No. CJ20130304.

[1]U. Ozgur, D. Hofstetter, and H. Morkoc, Proc. IEEE **98**, 1255 (2010).
[2]S. B. Ogale, Adv. Mater. **22**, 3125 (2010).
[3]J. M. Coey, M. Venkatesan, and C. B. Fitzgerald, Nature Mater. **4**, 173 (2005).
[4]W. Götz, N. M. Johnson, D. P. Bour, M. D. McCluskey, and E. E. Haller, Appl. Phys. Lett. **69**, 3725 (1996).
[5]W. Limmer, W. Ritter, R. Sauer, B. Mensching, C. Liu, and B. Rauschenbach, Appl. Phys. Lett. **72**, 2589 (1998).
[6]J. B. Wang, G. J. Huang, X. L. Zhong, L. Z. Sun, Y. C. Zhou, and E. H. Liu, Appl. Phys. Lett. **88**, 252502 (2006).
[7]H. Zhong, J. Wang, X. Chen, Z. Li, W. Xu, and W. Lu, J. Appl. Phys. **99**, 103905 (2006).
[8]B. Straumal, A. Mazilkin, S. Protasova, A. Myatiev, P. Straumal, G. Schütz, P. van Aken, E. Goering, and B. Baretzky, Phys. Rev. B **79**, 205206 (2009).
[9]D. C. Kundaliya, S. B. Ogale, S. E. Lofland, S. Dhar, C. J. Metting, S. R. Shinde, Z. Ma, B. Varughese, K. V. Ramanujachary, L. Salamanca-Riba, and T. Venkatesan, Nature Mater. **3**, 709 (2004).
[10]G. L. Liu, Q. Cao, J. X. Deng, P. F. Xing, Y. F. Tian, Y. X. Chen, S. S. Yan, and L. M. Mei, Appl. Phys. Lett. **90**, 052504 (2007).
[11]F. J. Manjón, B. Marí, J. Serrano, and A. H. Romero, J. Appl. Phys. **97**, 053516 (2005).
[12]R. Cuscó, E. Alarcón-Lladó, J. Ibáñez, L. Artús, J. Jiménez, B. Wang, and M. Callahan, Phys. Rev. B **75**, 165202 (2007).
[13]J. T. Ji, A. M. Zhang, T. L. Xia, Q. Cao, G. L. Liu, D. Hou, and Q. M. Zhang, Phys. Rev. B **82**, 014408 (2010).
[14]C. J. Cong, L. Liao, Q. Y. Liu, J. C. Li, and K. L. Zhang, Nanotechnology **17**, 1520 (2006).
[15]K. Samanta, S. Dussan, R. S. Katiyar, and P. Bhattacharya, Appl. Phys. Lett. **90**, 261903 (2007).
[16]M. A. Garcia, M. L. Ruiz-Gonzalez, A. Quesada, J. L. Costa-Kramer, J. F. Fernandez, S. J. Khatib, A. Wennberg, A. C. Caballero, M. S. Martin-Gonzalez, M. Villegas, F. Briones, J. M. Gonzalez-Calbet, and A. Hernando, Phys. Rev. Lett. **94**, 217206 (2005).
[17]C. B. Azzoni, M. C. Mozzati, P. Galinetto, A. Paleari, V. Massarotti, D. Capsoni, and M. Bini, Solid State Commun. **112**, 375 (1999).
[18]Q. Cao, S. He, Y. Deng, D. Zhu, X. Cui, G. Liu, H. Zhang, S. Yan, Y. Chen, and L. Mei, Curr. Appl. Phys. **14**, 744 (2014).
[19]S. Kolesnik and B. Dabrowski, J. Appl. Phys. **96**, 5379 (2004).
[20]T. C. Droubay, D. J. Keavney, T. C. Kaspar, S. M. Heald, C. M. Wang, C. A. Johnson, K. M. Whitaker, D. R. Gamelin, and S. A. Chambers, Phys. Rev. B **79**, 155203 (2009).
[21]A. Teke, Ü. Özgür, S. Doğan, X. Gu, H. Morkoç, B. Nemeth, J. Nause, and H. Everitt, Phys. Rev. B **70**, 195207 (2004).
[22]W. Y. Liang and A. D. Yoffe, Phys. Rev. Lett. **20**, 59 (1968).
[23]F. X. Xiu, Z. Yang, L. J. Mandalapu, and J. L. Liu, Appl. Phys. Lett. **88**, 152116 (2006).
[24]Z. Yang and J. L. Liu, J. Vacuum Sci. Technol. B **28**, C3D6 (2010).
[25]F. Jiang and J. Zhang, Appl. Phys. Lett. **98**, 181912 (2011).
[26]C. Klingshirn, Phys. Status Solidi B **71**, 547 (1975).
[27]Q. Wang, Q. Sun, P. Jena, and Y. Kawazoe, Phys. Rev. B **70**, 052408 (2004).
[28]K. R. Kittilstved, N. S. Norberg, and D. R. Gamelin, Phys. Rev. Lett. **94**, 147209 (2005).
[29]D. Rubi, J. Fontcuberta, A. Calleja, L. Aragonès, X. Capdevila, and M. Segarra, Phys. Rev. B **75**, 155322 (2007).
[30]X. Wang, J. Xu, X. Yu, K. Xue, J. Yu, and X. Zhao, Appl. Phys. Lett. **91**, 031908 (2007).
[31]A. F. Kohan, G. Ceder, D. Morgan, and C. G. Van de Walle, Phys. Rev. B **61**, 15019 (2000).
[32]A. Janotti and C. G. Van de Walle, Phys. Rev. B **76**, 165202 (2007).
[33]F. Tuomisto, V. Ranki, K. Saarinen, and D. C. Look, Phys. Rev. Lett. **91**, 205502 (2003).
[34]N. N. Lathiotakis and M. Menon, Phys. Rev. B **78**, 193311 (2008).
[35]A. N. Andriotis and M. Menon, Phys. Rev. B **87**, 155309 (2013).
[36]L. B. Duan, G. H. Rao, Y. C. Wang, J. Yu, and T. Wang, J. Appl. Phys. **104**, 013909 (2008).
[37]K. R. Kittilstved, W. K. Liu, and D. R. Gamelin, Nature Mater. **5**, 291 (2006).